PHYSICS

H-linear magnetoresistance in $NbSe_2$ due to impeded cyclotron motion

Arwin Kool[1,2]*, Davide Pizzirani[1,2], Paul Tinnemans[2], Steffen Wiedmann[1,2], Felix Flicker[3], Jasper van Wezel[4], Nigel E. Hussey[1,2,3]*, Roemer D. H. Hinlopen[3]*

Linear magnetoresistance (LMR) is a widespread phenomenon observed in a host of quantum materials ranging from semiconductor nanostructures to quantum critical and strange metals. While multiple scenarios to explain LMR have been proposed, a complete understanding of the phenomenon remains elusive. It is highly likely that the origin of LMR depends on the specific electronic state. Here, we report a study of the impact of disorder on the form of the magnetoresistance of the prototypical charge-density-wave (CDW) compound 2*H*-$NbSe_2$. The magnetoresistance is shown to exhibit strong qualitative and quantitative agreement with Boltzmann transport analysis incorporating impeded cyclotron motion (ICM). We identify the source of ICM in 2*H*-$NbSe_2$ as strong scattering sinks where the CDW order connects the high-temperature Fermi cylinders. Such unusual "hotspots" provide an explanation for the observed LMR as well as for the long-unexplained absence of quantum oscillations inside the charge-ordered state in 2*H*-$NbSe_2$. These findings provide strong evidence that ICM generates LMR in certain correlated metals.

INTRODUCTION

Linear-in-field magnetoresistance (LMR) contrasts markedly with the usual quadratic-to-saturating shape of the MR found in conventional metals. This, coupled with its remarkable robustness (extending over an anomalously broad field range) and its realization in a host of different quantum materials, from semiconductors (*1*, *2*) and Dirac semimetals (*3*) to quantum critical metals (*4*–*6*) and doped Mott insulators (*7*–*9*), has led to sustained interest in the LMR phenomenon for well over half a century. Reflecting the breadth of material classes in which LMR has been observed, multiple proposals have been put forward for its origin. The first category of proposals centers on materials with a low or vanishing carrier density. In GaAs quantum wells, for example, carrier density fluctuations result in a nonsaturating LMR up to high magnetic fields (*1*, *2*). For more strongly disordered semiconductors, LMR can arise from the formation of an effective random resistor network (*10*, *11*), while LMR is also expected at high magnetic field strengths near the quantum limit, where only a few Landau levels remain occupied (*12*). For metals with a high carrier density, LMR can arise, albeit over a limited field range, from sharp corners on the Fermi surface (FS) (*13*–*15*).

The manifestation of LMR in correlated metals with relatively simple, large, cylindrical FS geometries, however, suggests an alternative origin possibly linked to the emergence of novel electronic states. In iron-based superconductors tuned to their quantum critical point, for example, a peculiar form of nonsaturating H^2- to *H*-linear MR—with a *T*-independent slope—has been reported (*4*–*6*). The MR in these systems also exhibits a novel form of (non-Kohler) scaling in which magnetic field and temperature (rather than the zero-field resistivity) appear in quadrature (*4*). LMR with similar scaling properties has also been observed in the high-T_c cuprates, both close to the end of the pseudogap regime (*7*) and beyond (*8*, *9*). In the latter, the *T*-independent slope of the LMR is found to scale directly with both T_c and the coefficient of the low-*T* *T*-linear resistivity (*16*), suggesting a direct link to strange metallicity and high-T_c superconductivity.

The simplicity and robustness of the LMR found in the iron-based and cuprate superconductors have motivated a number of tailored theoretical proposals, including real-space binary distributions (*17*), real-space patches (*18*), carrier density fluctuations (*19*), and strong scattering sinks (*20*–*22*) among others. Proposals that incorporate scattering "hotspots" or any other obstruction to cyclotron motion on the FS can be generalized through the concept of impeded cyclotron motion (ICM) (*21*). In this picture, the orbital motion of carriers around the FS is truncated at specific loci, for example, through gapping, heavy effective masses, or intense scattering. These loci themselves are irrelevant for the resistivity of the material in the absence of a magnetic field due to shorting by the rest of the FS (which we will refer to as cold). With field applied, however, cyclotron motion of the cold carriers is impeded, resulting in a characteristic crossover from H^2- to *H*-linear MR with a slope that is *T* independent (*21*). The universality of LMR in correlated metals is then explained by the wide range of possible sources of the impedances that might occur, including hotspot scattering off antiferromagnetic spin fluctuations (*20*, *23*), van Hove singularities (*24*), static domains of glassy density-wave order (*22*), Fermi arcs in underdoped cuprates (*25*), or partial FS incoherence (*9*). Hence, identifying materials where ICM can account for the form and magnitude of the LMR as well as the range in tuning parameters where LMR is observed would provide definitive evidence of a dominant (and strongly *k*-dependent) interaction.

In this context, the prototypical charge-density-wave (CDW) compound 2*H*-$NbSe_2$ (henceforth abbreviated to $NbSe_2$) can be considered a viable candidate for the realization of ICM (*21*). Among the dichalcogenides, $NbSe_2$ has a relatively low CDW transition temperature of $T_{CDW} = 33$ K and a high superconducting transition temperature of $T_c = 7.2$ K. As shown in Fig. 1A, $NbSe_2$ is composed of Nb slabs sandwiched between Se atoms. LMR was first reported in $NbSe_2$ more than 50 years ago (*26*) and ascribed to magnetic breakdown through the gaps opened by the CDW (*27*). Such behavior, however, is known to result in MR saturation rather than LMR (*28*–*30*).

[1]High Field Magnet Laboratory (HFML-FELIX), Radboud University, Nijmegen, Netherlands. [2]Institute for Molecules and Materials, Radboud University, Nijmegen, Netherlands. [3]H. H. Wills Physics Laboratory, University of Bristol, Bristol, UK. [4]Institute for Theoretical Physics, University of Amsterdam, Amsterdam, Netherlands.
*Corresponding author. Email: arwin.kool@ru.nl (A.K.); n.e.hussey@bristol.ac.uk (N.E.H.); roemer.hinlopen@mpsd.mpg.de (R.D.H.H.)

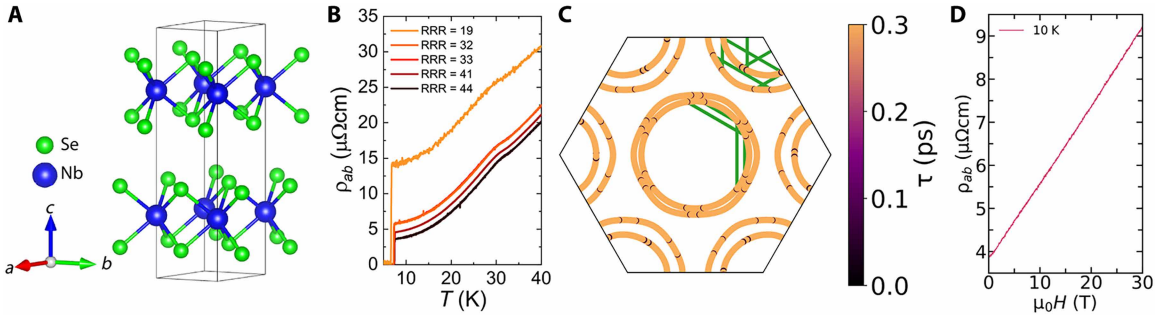

Fig. 1. Lattice, resistivity versus temperature, and simulation of the FS of bulk $NbSe_2$ in the CDW state. (**A**) Crystal structure of bulk 2*H*-$NbSe_2$. The crystal structure consists of two weakly coupled, hexagonal Se-Nb-Se layers. (**B**) In-plane resistivity $\rho_{ab}(T)$ for five samples of $NbSe_2$ of varying quality as indicated by the factor-of-four variation in the residual resistivity ρ_0. The superconducting and CDW transition temperatures decrease monotonically with increasing ρ_0 [decreasing residual resistivity ratio or RRR, consistent with previous disorder studies (*37*, *38*)]. (**C**) The tight-binding FS of bulk $NbSe_2$ previously determined via ARPES (*35*). Unless mentioned otherwise, we ignore the small pancake-shaped pocket centered around the Γ-point. Instead of a FS reconstruction, impedances (black) are shown where the FS is connected intrapocket by the CDW $\vec{Q}$-vector (examples in green), while cold charge is colored orange. (**D**) Exemplary LMR measured on the sample with RRR = 44 at $T = 10$ K.

The lack of quantum oscillations (QOs) from all pockets which participate in the CDW order also remains notable and unexplained (*31*, *32*). However, if the CDW order manifests with a large imaginary self-energy for any reason (e.g., low single-particle lifetimes for phonon-dressed quasiparticles), then the resulting impedances to cyclotron motion could explain both a lack of QOs on the participating pockets and the emergence of LMR which disappears with increasing temperature or pressure in tandem with the CDW phase (*33*).

To test the applicability of ICM to $NbSe_2$, we have carried out a magnetotransport study of bulk $NbSe_2$ over an unprecedented field range as a function of temperature and disorder. The LMR is found to disappear upon approach to the CDW transition temperature from below and, to within our experimental accuracy, follows Kohler scaling up to this breakdown temperature. Recall that Kohler scaling is a single-parameter scaling of the magnetoresistance with $\omega_c\tau$ (*34*) that is expected semiclassically if the MR changes solely due to a T-dependent scattering rate. Kohler scaling is obeyed in most elemental metals but can be violated, for instance, through changes in anisotropy or in the size of the FS, by a field dependence of the anisotropy or of the scattering rate, through changes in the effective mass and by changes in the mobility ratio between different pockets. Furthermore, no QOs have been observed in the cleanest crystals up to the highest field strength (30 T) and down to lowest temperatures (0.35 K). Using the known FS of $NbSe_2$ (*35*) and a single degree of freedom (the zero-field scattering rate determined by impurity scattering), we are able to explain the absence of QOs and model the presence of the LMR within the ICM framework. The slope of the H-linear MR agrees quantitatively with the model's prediction, while Kohler scaling and the temperature and disorder independence of the LMR slope are also reproduced. For completeness, limitations of the model and effects beyond the relaxation time approximation are also discussed.

RESULTS

Disorder dependence of the high-field MR of $NbSe_2$

Figure 1B shows the low-T $\rho(T)$ curves for five single crystals of $NbSe_2$ with a fourfold variation in their residual resistivity $\rho_0 = \rho(T_c)$. As reported in previous disorder studies, both T_c and T_{CDW} are found to drop with increasing ρ_0 (*36*–*39*). The CDW opens gaps primarily where parts of the FS are connected by the CDW wave vector $\vec{Q}$ within an individual pocket and most strongly on the inner K- and K'-barrels (*40*–*42*). The ICM hypothesis applied to $NbSe_2$ is that where such gaps open, additional sharp drops in the transport lifetime τ are experienced by the quasiparticles (Fig. 1C). This drop in lifetime is assumed to scale with the strength of the CDW order, disappearing at the CDW transition. An exemplar LMR within the CDW phase is shown in Fig. 1D. Below, we use the FS previously determined via angle-resolved photoemission spectroscopy (ARPES) (*35*) and this scattering lifetime to model the MR of $NbSe_2$ using a Boltzmann transport calculation. In addition, to investigate specific limitations of the model, we present calculations that include the proposed FS reconstruction as well as calculations that go beyond the relaxation time approximation.

Figure 2A shows a representative set of ρ_{ab} measurements as a function of applied magnetic field for the sample with RRR = 44, where RRR = ρ_{ab}(RT)/$\rho_{ab}(T_c)$. At the lowest temperatures and beyond a magnetic field strength large enough to suppress superconductivity, we observe H-linearity up to 30 T. Between T_c and 15 K, we observe a H^2- to H-linear crossover in the MR with a small crossover scale H^* between 0.5 and 1.0 T. Above 15 K, the H-linearity gradually breaks down, and then above T_{CDW}, the MR almost vanishes and exhibits more conventional quadratic-to-saturating behavior. Correspondingly, the Hall effect (see fig. S1) is temperature independent and electron-like below 15 K, changes sign at 25 K, and recovers the expected hole-like linear Hall response above ~40 K. At low-T, the H-linear slope is independent of temperature and has a value of ≈0.18 μΩcm/T (see Fig. 2B). This compares with previous literature values of 0.10 (*43*) and 0.13 μΩcm/T (*27*).

Figure 2C shows $\Delta\rho_{ab}$ [= $\rho_{ab}(\mu_0 H) - \rho_{ab}(0)$] of the five measured samples at $T = 10$ K. (The full dataset for all samples can be found in fig. S1). The H-linear slope of the MR is found to vary by ±3% despite a fourfold variation in ρ_0. To properly test Kohler scaling, the H^2-part of the MR should also collapse, which is obscured in Fig. 2C due to the low field scale of the turnover. We therefore performed a low-field study on crystals cut from the same mother crystals as the high field samples but with slightly different RRRs, to test specifically whether the quadratic part of the MR curves follows any type of scaling. The full dataset of these measurements is presented in figs. S2 and S3. We show the Kohler plot of these samples measured at $T = 10$ K in Fig. 2D. In

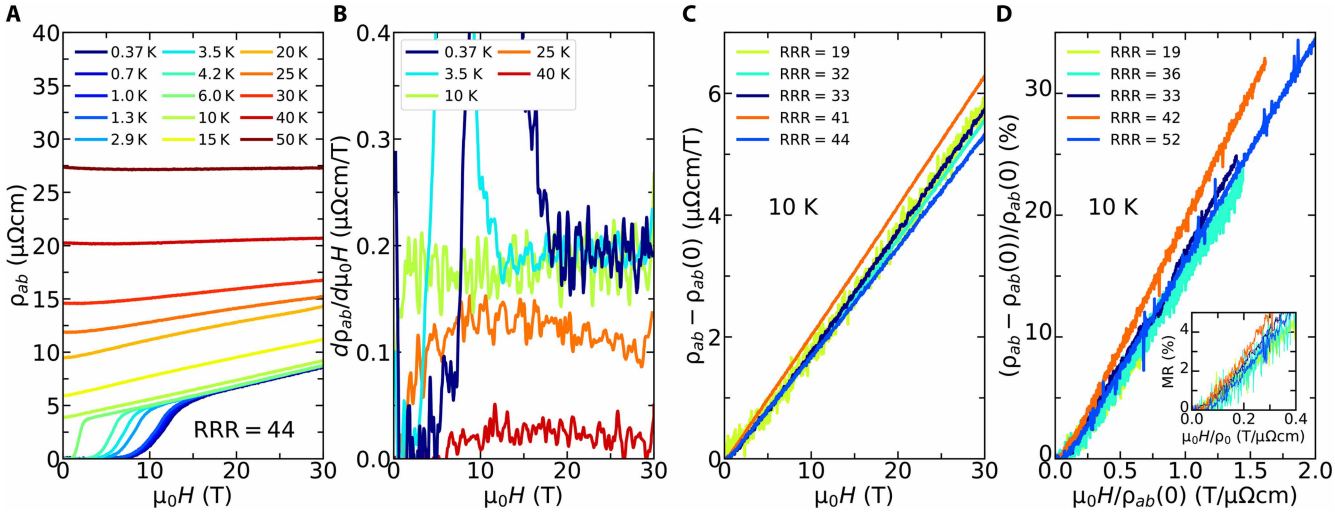

Fig. 2. Overview of the magnetoresistance behavior in 2*H*-$NbSe_2$. (**A**) Raw MR data for the sample with the largest RRR measured between 0.37 and 50 K. The current is applied along the *a* axis, and the magnetic field is oriented in the *c* direction. We observe a clear *H*-linear MR over an extended field range below 15 K. Above 15 K, the magnitude decreases until the MR effectively vanishes at 50 K. (**B**) Field derivative of the resistivity $d\rho_{ab}/d\mu_0 H$ reveals a robust nonsaturating, *T*-independent LMR below $T = 15$ K that persists up to the highest magnetic fields. Above 15 K, the MR develops a tendency toward saturation. (**C**) MR curves obtained just above T_c (at 10 K) in the crystals whose zero-field resistivity is shown in Fig. 1B. The high field MR is clearly linear, while the low field MR shows a more quadratic character. The field range of the quadratic behavior depends on the RRR. (**D**) Kohler plot for field sweeps made up to 8 T of crystals cut from the same mother crystals as the high-field samples but with slightly different RRRs. Kohler scaling is obeyed at 10 K as a function of disorder. Inset: zoom of the low-field quadratic part of the MR, showing the robustness of the scaling.

the inset of Fig. 2D, we also show a blow-up of the same Kohler plot, focusing on the low-field response. As can be seen, the curves collapse to within experimental error, implying that the MR in $NbSe_2$ does obey Kohler scaling. In the following section, we proceed to model the data to better understand the origin of the LMR in $NbSe_2$.

Modeling the data using ICM

ICM provides a phenomenological description of MR that is insensitive to the microscopic details. This allows us to thoroughly test the model against the experimental data with few degrees of freedom. We follow (*21*) and hypothesize that the predominant effect of the CDW order on the electron dynamics is to turn points on the FS connected by a CDW $\vec{Q}$-vector incoherent or, equivalently, to enlarge their imaginary self-energies into a set of hotspots. The suppression of the carrier lifetime at the hotspots then scales with the strength of the CDW order and impedes cyclotron motion, suppressing QOs and generating LMR.

Even at $\mu_0 H = 30$ T and $T = 0.35$ K, QOs associated with the major pockets (with predicted frequencies of 5 to 10 kT) are absent. Under these conditions, they would be expected to trace out a real-space orbit of typical cyclotron radius $R_c \approx 75$ nm based on the known FS of $NbSe_2$. This is in stark contrast with the pancake pocket, which has been observed at 2.5 T when $R_c = 225$ nm despite being subject to additional scattering in the vortex liquid state (*31*, *32*). We similarly observe QOs from the pancake pocket when we rotate the magnetic field (see fig. S5). The cyclotron radius of the smallest pockets of $NbSe_2$ after backfolding and hybridization is expected to be as small as $R_c \approx 8$ nm in our experimental conditions (see the Supplementary Materials for details), yet no QOs are observed in these either. This notable lack of QOs supports the notion that the CDW order in 2*H*-$NbSe_2$ forms impedances at specific positions in *k*-space, preventing electrons from completing cyclotron orbits anywhere on the FS (except around the pancake pocket that of itself does not participate in the CDW order).

To test this hypothesis more rigorously, we develop a phenomenological magneto-transport model using the minimal tight-binding expansion of the FS of $NbSe_2$ (*35*). Backfolding and hybridization undoubtedly occur, but by themselves do not explain the observations and so we neglect these steps initially to focus on the essential ingredients required to explain both the MR and the absence of QOs. Impedances are placed at locations at which the CDW $\vec{Q}$-vector connects the FS, only keeping intrapocket connections in accordance with (*40*) and noting that the spectral weight observed at other locations on the FS in ARPES remains unchanged (*35*, *44*). The impedances are modeled as locally suppressed lifetimes as shown in Fig. 1C. We use the lifetime for its computational simplicity but emphasize that the results are valid also if the impedances result, e.g., from a removal of spectral weight away from the Fermi energy or from high local effective masses; in all cases, the contribution of the impedances themselves to the total conductivity is negligible (due to shorting effects) and affects the magnetotransport solely by ICM. We use the full Shockley-Chambers tube integral formalism (SCTIF) of the Boltzmann transport equation assuming the relaxation time approximation and neglecting *c*-axis dispersion (*45*, *46*). The only degree of freedom in the model is the isotropic cold scattering time τ across the FS, which we fit to the zero-field resistivity $\rho_{ab}(0)$.

We start with the most general solution to the Boltzmann transport equation within the relaxation time approximation and without thermal broadening. The resulting formula within the SCTIF is (*45*, *46*)

$$\sigma_{ij} = \frac{e^2}{\pi\hbar}\int_{FS}\frac{d^2\vec{k}}{(2\pi)^2}\frac{v_i}{v}\int_0^\infty dt\, v_j(-t)\exp\left[-\int_0^t \frac{dt'}{\tau(-t')}\right] \quad (1)$$

Here, σ is the conductivity, indices *i,j* run over *x,y* (the k_z corrugation of the FS is neglected), *e* is the electron charge, $\hbar$ is the reduced Planck's constant, FS is the FS including a sum over the different pockets, τ is the velocity relaxation time, and $\vec{v} := \frac{1}{\hbar}\vec{\nabla}_{\vec{k}}\varepsilon_{\vec{k}}$ is the Fermi velocity defined through the energy dispersion ε_k. The $\vec{k}$ dependence of $\vec{v}$ and τ is implicit for clarity. Time dependence manifests through cyclotron motion, i.e., through $\vec{k}(t)$. The exponent in Eq. 1 is the probability for a quasiparticle to survive to time *t*. The integrals can be evaluated for arbitrary magnetic field strengths. Temperature dependence arises solely from the *T* dependence of τ. Resistivity is obtained through a full matrix inversion of σ. The model is defined entirely by ε_k and $\tau(\vec{k})$. We take ε_k from a previous tight-binding fit to ARPES data which contains exactly one hole per unit cell while neglecting the selenium pancake pocket (*35*). $\tau(k)$ is shown in Fig. 1C for the entire FS and in Fig. 3D for an individual hotspot.

In Fig. 3 (A and B), we directly compare the simulations obtained from our simple model to the experimental data obtained on the sample with RRR = 44. For clarity, we only include curves at *T* = 10 and 25 K. As shown in Fig. 3B at *T* = 10 K, the model generates a robust LMR with a slope of 0.11 μΩcm/T that persists up to the highest fields used in our study. Consistent with the data shown in Fig. 2C, this *H*-linear slope is independent of τ ($\rho_{ab}(0)$). Despite the lack of tunability, the model captures well the crossover field H^* and reproduces the magnitude of the MR to within 30%.

The LMR slope in ICM is nominally inversely proportional to the cold carrier density (akin to the traditional Hall effect) and robust against changes in scattering time, temperature, disorder, or effective mass as observed experimentally. Upon increasing temperature, the CDW gap decreases, and as a result, the impedances are expected to disappear. Consistent with ICM, the LMR is suppressed near T_{CDW}. The experimentally observed MR essentially vanishes at 50 K, and the observed and modeled Hall effect matches with expectations from the carrier density (see the Supplementary Materials for details). In the intermediate temperature range just below T_{CDW}, we anticipate the CDW order to be sufficiently weak that carriers are affected by the CDW, but their cyclotron motion may not be effectively impeded. (Note that given the estimated effective mass in $NbSe_2$, this temperature is too high for QOs to be observed.) To incorporate this effect, we introduce a second degree of freedom by artificially weakening the impedances such that magnetic breakdown is possible within the experimentally observable regime. This means that the hotspots are not infinitely strong and there remains a finite probability $\exp(-B_{br}/B)$ for charge to maintain cyclotron motion across the impedance. At low *T*, the breakdown field B_{br} is much greater than 50 T and decreases toward T_{CDW}. The result for *T* = 25 K is shown in Fig. 3 (A and B) and reproduces the observations: The MR diminishes in size and saturates in tandem. In other words, the robust LMR has vanished. Note that the tendency of the MR in $NbSe_2$ to saturate already at intermediate temperatures is unusual yet is well reproduced by the ICM model. Recent results at low *T* as a function of hydrostatic pressure show that the MR similarly diminishes together with the CDW order (*33*). Collectively, these experimental observations appear to tie the LMR to the CDW order, which is naturally explained by impedances which scale with the CDW order parameter as adopted here. Last, the model naturally reproduces Kohler scaling at low *T* where the isotropic cold scattering rate is the only temperature-dependent parameter.

The turnover scale H^* where LMR sets in represents the magnetic field at which cold quasiparticles can traverse between hotspots via cyclotron motion. For this process, we expect the Kohler relation $H^* \propto \rho(0)$ to hold both as a function of temperature (below ~⅔ T_{CDW} when impedances appear to be well established and breakdown seems absent) as well as disorder. This relationship, shown in Fig. 3C, agrees well with the model predictions. In the Supplementary Materials, we present a version of the model that also fits the result in absolute units for all temperatures, magnetic fields, and disorder values by incorporating not only the cold scattering rate but also the width and strength of hotspots to account for magnetic breakdown.

Despite its successes, this simple model has some shortfalls that we summarize here while referring the reader to the Supplementary Materials for more details. First and foremost, although ICM describes a simultaneous *H*-linearity in the MR and Hall effect, the sign change in the Hall effect which sets in simultaneously with the LMR remains unexplained. Second, the model relies on the relaxation time approximation and thus neglects contributions to the conductivity from nonzero averaged velocities near the hotspots (*47*). To address

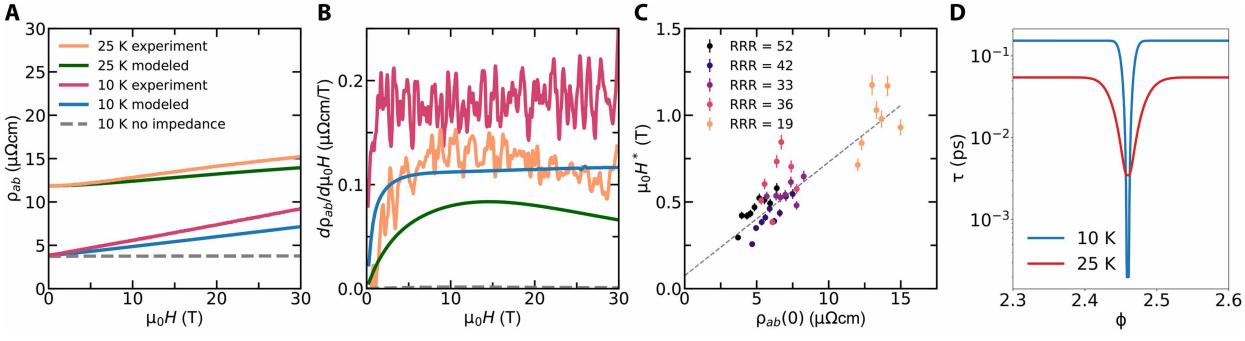

Fig. 3. Comparison of the ICM model to the measured data. (**A**) Comparison of the modeled MR response (blue) to the measured data (purple) on the RRR = 44 sample at *T* = 10 K, i.e., well within the *H*-linear regime. The modeled response without impedances (gray) indicates that the MR originates from the impedances and not from the FS itself. A second comparison (green and orange, respectively) is shown at *T* = 25 K (close to T_{CDW}) where we observe a breakdown of *H*-linearity. This breakdown at high magnetic field can be reproduced by artificially weakening the hotspots such that quasiparticles have a finite probability for breakdown (see the Supplementary Materials for details. (**B**) The derivatives of the curves shown in (A) highlight the linearity and turnover scale. Overall, the model shows good qualitative and reasonable quantitative agreement with the data. (**C**) H^* versus $\rho_{ab}(0)$ obtained by varying both disorder and temperature between 8 and 18 K. Here, H^* is extracted as the field value where the derivative $d\rho_{ab}/d\mu_0 H$ reaches 90% of the high-field linear slope. The gray dashed line is a guide to the eye. (**D**) Representative impedances at 10 and 25 K. ϕ refers to the azimuthal angle on the inner Γ pocket. By weakening impedances with increasing temperature toward T_{CDW}, the observed MR saturation is captured.

these points, we consider in the Supplementary Materials various extensions to the model that include the full FS reconstruction, additional anisotropy in the reconstructed phase from interpocket and interband interactions, and a practical Boltzmann transport framework beyond the relaxation time approximation that was previously applied to quasi–one-dimensional conductors in (*48*). First, we find that the Peierls reconstruction without impedances is insufficient to explain the absence of QOs or the presence of LMR in $NbSe_2$. Second, we address any concerns about charge conservation within ICM by developing a fully charge conserving model. Last, we find evidence beyond the relaxation time approximation which favors impedances due to reduced quasiparticle coherence (e.g., through high imaginary self-energy or spectral weight shifted away from the FS) over scattering origins (e.g., domain wall scattering). We stress, however, that further work is necessary to establish the precise microscopic origin of ICM in $NbSe_2$.

DISCUSSION

Comprehensive measurements of the temperature, magnetic field, and disorder dependence of the MR in $NbSe_2$ confirm the robustness of the LMR and the concomitant lack of QOs up to higher field strengths (30 T) and down to lower temperatures (0.35 K) than previously reported. Both phenomena have remained unexplained for 50 years. Our minimal ICM model, adapted to the known FS of $NbSe_2$, is found to offer a coherent explanation for the robust LMR up to the highest field strength, its magnitude, its onset field H^*, the vanishing of the MR above T_{CDW}, the saturation of the MR in the intermediate temperature range, its disappearance under hydrostatic pressure, the disorder independence of the *H*-linear slope, Kohler scaling, the simultaneous linearity of the Hall effect, and the absence of QOs on all pockets except the selenium pancake pocket. The only failure of the model in its current form is its inability to account for the sign change in the Hall effect, which may result from the lack of FS reconstruction in the model.

As highlighted in Introduction, multiple scenarios have been proposed to explain LMR, and the origin of LMR in a particular metal is likely to depend on the specifics of their electronic state. Before discussing the implications of our modeling for the physics of $NbSe_2$, therefore, we first describe here what aspects of the data are inconsistent with other models for the *H*-linear MR. While the nonlinear $\rho_{yx}(H)$ in $NbSe_2$ hints at multiple carriers, no variant of the multiband Drude model can generate such a robust *H*-linear MR. Models based on random resistor networks (*10*, *49*) or fluctuations in the carrier density (*2*, *19*) can also be ruled out since (i) $\Delta\rho$ is *H*-linear while ρ_{yx} is nonlinear, and (ii) at low *T*, the magnitude of the MR is essentially constant while ρ_{yx} changes sign. At the same time, a different disorder dependence would be expected. Previous scanning tunneling microscopy work revealed that CDW domains in $NbSe_2$ shrink with increased disorder down to ~5 nm in strongly disordered crystals (*50*). This is expected to enhance the mobility variance and thereby markedly increase the LMR (*49*, *51*), in contrast with the experimental findings (see Fig. 2). Additional assumptions or degrees of freedom would be required for the random resistor network picture to capture all the experimental observables captured by the ICM model. The low field scale for the crossover *H*-linear MR (~1 T) implies that the quantum model of Abrikosov (*12*) is not relevant here. Moreover, the hotspot model of Koshelev (*20*) predicts $\rho_{yx} \sim H^2$, while the notion that sharp FS corners account for the *H*-linear MR, as proposed for other CDW compounds (*15*), appears invalid since the robustness of the *H*-linearity up to 30 T implies extremely sharp FS corners and thus reconstruction into smaller pockets, for which one should observe (*13*) QOs and MR saturation well below 30 T in clean $NbSe_2$—inconsistent with our results. Last, the robust H/T MR scaling behavior seen in several strange (*9*) and quantum critical (*4*, *6*) metals indicates that its origin in those systems is tied to the *T*-linear resistivity. In $NbSe_2$, by contrast, LMR is observed in a regime where the resistivity does not exhibit *T* linearity.

In the original Peierls picture of CDW order (*52*), nesting of the FS by a wave vector $\vec{Q}$ yields a divergence of the electronic susceptibility. In the presence of even infinitesimal electron-phonon coupling, this is accompanied by a sharp dip (Kohn anomaly) in the phonon dispersion causing a combined electronic and lattice instability and reconstruction of the FS (*53*). In this idealized scenario, there is no additional scattering in the hybridized FS after backfolding, beyond the usual isotropic impurity scattering. In practice, perfect nesting does not exist (*54*). In $NbSe_2$, in particular, the applicability of the ideal Peierls picture has long been questioned. It cannot predict the observed CDW vector (*55*), the broad Kohn anomaly (*56*), nor the presence of fluctuations above T_{CDW}. Models of the CDW order instead require a momentum dependence of the electron-phonon coupling and inelastic processes away from the Fermi level (*41*, *56*, *57*). Our study suggests that impedances to cyclotron motion are an essential extra ingredient to explain both the LMR and the lack of QOs. Last, a scenario based on hotspots formed through strong scattering from (CDW) quantum fluctuations, i.e., due to proximity to a quantum critical point (*4*), seems unlikely here. Thermal variations of the CDW order parameter should be present above T_{CDW}, be strongest near T_{CDW}, and be suppressed at lower *T* (*33*, *56*). The LMR in $NbSe_2$, meanwhile, is absent above T_{CDW}, shows breakdown just below T_{CDW}, and is strongest at low *T*.

An alternative type of fluctuation may lie in the strong coupling nature of the CDW formation (*58*, *59*). Going beyond the idealized Peierls picture, quantitative modeling of the CDW requires renormalizing the bare electrons and phonons with fluctuations beyond the mean field level (*40*, *41*). This results in a strongly momentum-dependent CDW gap but may equally affect the off-diagonal elements of the gap matrix, which determine the lifetime of renormalized electrons. Under the natural assumption that the momentum dependence of the diagonal and off-diagonal elements track one another, the scattering rate is largest at hotspots along the FS connected by CDW wave vectors.

Another possibility is that impedances are formed by scattering from CDW domain walls. Traversing a sharp domain wall can be thought of as quenching from one CDW structure to one shifted by a single lattice spacing. Bloch's theorem implies that spatially shifting the electronic wave functions adds a momentum-dependent phase factor. For electronic states at hotspots along the FS, the phase shift is guaranteed to yield different electronic states at the FS. The joint density of states available for scattering from CDW domain walls is thus maximized at hotspots, causing their scattering rate to be maximized. Note that although domain sizes larger than the expected cyclotron size at 30 T have been observed in clean $NbSe_2$ (see also the Supplementary Materials) (*50*), these do not account for phase slip lines in individual CDW components attached to point defects. The density of such phase slips is determined by the difference between the locally commensurate CDW vector and the incommensurate position of the peak in electronic susceptibility (*40*, *60*, *61*) and may thus be expected to be relatively large and doping independent.

Estimating the CDW correlation length to be $\xi \leq 50$ nm and using ARPES results for the CDW gap anisotropy (*35*), the inequality $\Delta_{CDW} < \hbar v_F/\xi$ is found to hold for all major FS pockets except for the inner *K* barrel on which the CDW order is strongest. In this regime, it has been suggested that FS reconstruction may be inhibited since the CDW appears glassy to the electrons (*22*). In underdoped cuprates, this inequality is also satisfied, and yet QOs of reconstructed Fermi pockets have been observed (*62*, *63*). More work is required to thoroughly test this mechanism. Last, we point out that two key ARPES studies on $NbSe_2$ (*35*, *44*) show a reduction or even vanishing of the quasiparticle spectral weight at the CDW hotspots. At the same time, the backfolded spectral weight is minimal. Certainly, the origin of the impedances found here appear related to the ARPES results. Neither ARPES nor LMR, however, can by themselves reveal the microscopic origin of the spectral weight reduction nor the impedances. Resolving this will require further investigation.

Overall, our study provides indirect but robust evidence for the formation of impedances alongside the usual FS reconstruction in the CDW ordered phase of $NbSe_2$. The prototypical nature of $NbSe_2$ among (strongly coupled) density wave systems, both charge and spin, indicates that this result may have broader implications. Considering the pnictides (where hotspots from critical spin fluctuations may act as impedances) and optimally doped cuprates (where the edges of Fermi arcs offer a natural source of impedance), the turnover scale of the MR appears entirely insensitive to disorder and scales with H/T, indicative of some form of strange metallic transport possibly beyond the relaxation time approximation. Nevertheless, these examples illustrate that impedances naturally emerge across strongly correlated electron systems through the *k*-selectivity of a wide variety of correlation effects with distinctive consequences in the presence of a magnetic field (*21*). Understanding how ICM affects the relatively simple Fermi-liquid $NbSe_2$ is essential if we are to understand related phenomena in more complex unconventional superconductors.

We conclude by arguing that ICM enables a deeper and simpler understanding of the electrical transport and lack of QOs in $NbSe_2$ than is possible via the conventional FS reconstruction scenario. While further work is required to identify the microscopic origin of ICM in $NbSe_2$, the ICM scenario presented here offers a promising starting point toward a new paradigm for describing density wave order and correlated electron dynamics.

MATERIALS AND METHODS

Bulk 2*H*-$NbSe_2$ crystals of varying quality, indicated by a varying T_c and RRR, were obtained from the crystal provider HQ Graphene and cut into bar shapes along the *a* or *b* axis using a razor blade. X-ray diffraction (XRD) measurements indicated that there were no impurity phases present to within experimental resolution present. We tentatively ascribe the disorder to crystal imperfections (e.g., dislocations), point-like impurities, and vacancies created during the growth process. XRD was also used to determine the crystallographic orientation of each crystal. [The crystal structure itself, shown in Fig. 1, was generated using VESTA (*64*)]. Electrical contacts were made in a six-probe Hall bar configuration by fixing 25-μm-diameter gold wires to the sides of the samples using 4929N DuPont silver paste, carefully shorting out the *c* axis to avoid contributions from the out-of-plane resistivity ρ_c. Note that the data for the RRR = 19 sample in Fig. 2D) are noisier due to a contact that slightly degraded during the experiment. High-field transport properties were measured in a laboratory-built ^{3}He system inserted into a 30 T Bitter magnet at the HFML-FELIX using a Keithley 6221 current source and a Stanford Research SR865 lock-in amplifier. The derivatives shown in Fig. 2 were smoothed with a Savitsky-Golay filter of polynomial order 1. Low-field measurements were performed in a Cryogenics cryogen-free measurement system. Modeling was performed using a Python code (see the Supplementary Materials for details).

Supplementary Materials

This PDF file includes:

Supplementary Text
Figs. S1 to S14
Tables S1 and S2
References

REFERENCES

1. C. Herring, Effect of random inhomogeneities on electrical and galvanomagnetic measurements. *J. Appl. Phys.* **31**, 1939–1953 (1960).
2. T. Khouri, U. Zeitler, C. Reichl, W. Wegscheider, N. E. Hussey, S. Wiedmann, J. C. Maan, Linear magnetoresistance in a quasifree two-dimensional electron gas in an ultrahigh mobility GaAs quantum well. *Phys. Rev. Lett.* **117**, 256601 (2016).
3. K. K. Huynh, Y. Tanabe, K. Tanigaki, Both electron and hole Dirac cone states in $Ba(FeAs)_2$ confirmed by magnetoresistance. *Phys. Rev. Lett.* **106**, 217004 (2011).
4. I. M. Hayes, R. D. McDonald, N. P. Breznay, T. Helm, P. J. W. Moll, M. Wartenbe, A. Shekhter, J. G. Analytis, Scaling between magnetic field and temperature in the high-temperature superconductor $BaFe_2(As_{1-x}P_x)_2$. *Nat. Phys.* **12**, 916–919 (2016).
5. N. Maksimovic, I. M. Hayes, V. Nagarajan, J. G. Analytis, A. E. Koshelev, J. Singleton, Y. Lee, T. Schenkel, Magnetoresistance scaling and the origin of *H*-linear resistivity in $BaFe_2(As_{1-x}P_x)_2$. *Phys. Rev. X* **10**, 041062 (2020).
6. S. Licciardello, N. Maksimovic, J. Ayres, J. Buhot, M. Čulo, B. Bryant, S. Kasahara, Y. Matsuda, T. Shibauchi, V. Nagarajan, J. G. Analytis, N. E. Hussey, Coexistence of orbital and quantum critical magnetoresistance in $FeSe_{1-x}S_x$. *Phys. Rev. Res.* **1**, 023011 (2019).
7. P. Giraldo-Gallo, J. A. Galvis, Z. Stegen, K. A. Modic, F. F. Balakirev, J. B. Betts, X. Lian, C. Moir, S. C. Riggs, J. Wu, A. T. Bollinger, X. He, I. Božović, B. J. Ramshaw, R. D. McDonald, G. S. Boebinger, A. Shekhter, Scale-invariant magnetoresistance in a cuprate superconductor. *Science* **361**, 479–481 (2018).
8. T. Sarkar, P. R. Mandal, N. R. Poniatowski, M. K. Chan, R. L. Greene, Correlation between scale-invariant normal-state resistivity and superconductivity in an electron-doped cuprate. *Sci. Adv.* **5**, eaav6753 (2019).
9. J. Ayres, M. Berben, M. Čulo, Y.-T. Hsu, E. van Heumen, Y. Huang, J. Zaanen, T. Kondo, T. Takeuchi, J. R. Cooper, C. Putzke, S. Friedemann, A. Carrington, N. E. Hussey, Incoherent transport across the strange-metal regime of overdoped cuprates. *Nature* **595**, 661–666 (2021).
10. M. Parish, P. Littlewood, Non-saturating magnetoresistance in heavily disordered semiconductors. *Nature* **426**, 162–165 (2003).
11. Z. H. Wang, L. Yang, X. J. Li, X. T. Zhao, H. L. Wang, Z. D. Zhang, X. P. A. Gao, Granularity controlled nonsaturating linear magnetoresistance in topological insulator Bi_2Te_3 films. *Nano Lett.* **14**, 6510–6514 (2014).
12. A. A. Abrikosov, Quantum magnetoresistance. *Phys. Rev. B* **58**, 2788–2794 (1998).
13. A. B. Pippard, *Magnetoresistance in metals*, Cambridge Studies in Low Temperature Physics (Cambridge Univ. Press, 1989).
14. A. E. Koshelev, Linear magnetoconductivity in multiband spin-density-wave metals with nonideal nesting. *Phys. Rev. B* **88**, 060412 (2013).
15. Y. Feng, Y. Wang, D. M. Silevitch, J.-Q. Yanc, R. Kobayashi, M. Hedo, T. Nakama, Y. Onuki, A. V. Suslov, B. Mihaila, P. B. Littlewood, T. F. Rosenbaum, Linear magnetoresistance in the low-field limit in density-wave materials. *Proc. Natl. Acad. Sci. U.S.A.* **116**, 11201–11206 (2019).
16. J. Ayres, M. Berben, C. Duffy, R. D. H. Hinlopen, Y.-T. Hsu, A. Cuoghi, M. Leroux, I. Gilmutdinov, M. Massoudzadegan, D. Vignolles, Y. Huang, T. Kondo, T. Takeuchi, S. Friedemann, A. Carrington, C. Proust, N. E. Hussey, Universal correlation between *H*-linear magnetoresistance and *T*-linear resistivity in high-temperature superconductors. *Nat. Commun.* **15**, 8406 (2024).
17. C. Boyd, P. W. Phillips, Single-parameter scaling in the magnetoresistance of optimally doped $La_{2-x}SrxCuO_4$. *Phys. Rev. B* **100**, 155139 (2019).
18. A. A. Patel, J. McGreevy, D. P. Arovas, S. Sachdev, Magnetotransport in a model of a disordered strange metal. *Phys. Rev. X* **8**, 021049 (2018).

19. J. Singleton, Temperature scaling behavior of the linear magnetoresistance observed in high-temperature superconductors. *Phys. Rev. Mater.* **4**, 061801 (2020).
20. A. E. Koshelev, Magnetotransport of multiple-band nearly antiferromagnetic metals due to hot-spot scattering. *Phys. Rev. B* **94**, 125154 (2016).
21. R. D. H. Hinlopen, F. A. Hinlopen, J. Ayres, N. E. Hussey, B^2 to B-linear magnetoresistance due to impeded orbital motion. *Phys. Rev. Res.* **4**, 033195 (2022).
22. J. Kim, E. Altman, S. Chatterjee, Linear magnetoresistance from glassy orders. *Proc. Natl. Acad. Sci. U.S.A.* **121**, e2405720121 (2024).
23. C. M. Duffy, S. J. Tu, Q. H. Chen, J. S. Zhang, A. Cuoghi, R. D. H. Hinlopen, T. Sarkar, R. L. Greene, K. Jin, N. E. Hussey, Evidence for spin-fluctuation-mediated superconductivity in electron-doped cuprates. arXiv:2502.13612 [cond-mat.supr-con] (2025).
24. G. Grissonnanche, Y. Fang, A. Legros, S. Verret, F. Laliberté, C. Collignon, J. Zhou, D. Graf, P. A. Goddard, L. Taillefer, B. J. Ramshaw, Linear-in temperature resistivity from an isotropic Planckian scattering rate. *Nature* **595**, 667–672 (2021).
25. M. R. Norman, H. Ding, M. Randeria, J. C. Campuzano, T. Yokoya, T. Takeuchik, T. Takahashi, T. Mochiku, K. Kadowaki, P. Guptasarma, D. G. Hinks, Destruction of the Fermi surface in underdoped high-T_c superconductors. *Nature* **392**, 157–160 (1998).
26. R. C. Morris, R. V. Coleman, R. Bhandari, Superconductivity and magnetoresistance in $NbSe_2$. *Phys. Rev. B* **5**, 895–901 (1972).
27. M. Naito, S. Tanaka, Galvanomagnetic effects in the charge-density-wave state of 2*H*-$NbSe_2$ and 2*H*-$TaSe_2$. *J. Phys. Soc. Jpn.* **51**, 228–236 (1982).
28. L. M. Falicov, P. R. Sievert, Theory of the galvanomagnetic effects in metals with magnetic breakdown: Semiclassical approach. *Phys. Rev.* **138**, A88–A98 (1965).
29. A. B. Pippard, Quantization of coupled orbits in metals: II. The two-dimensional network, with special reference to the properties of zinc. *Philos. Trans. A Math Phys. Eng. Sci.* **256**, 317–355 (1964).
30. A. B. Pippard, Magnetic breakdown in a dislocated lattice. *Proc. A* **287**, 165–182 (1965).
31. J. E. Graebner, M. Robbins, Fermi-surface measurements in normal and superconducting 2*H*-$NbSe_2$. *Phys. Rev. Lett.* **36**, 422–425 (1976).
32. R. Corcoran, P. Meeson, Y. Onuki, P.-A. Probst, M. Springford, K. Takita, H. Harima, G. Y. Guo, B. L. Gyorffy, Quantum oscillations in the mixed state of the type II superconductor 2*H*-$NbSe_2$. *J. Phys. Condens. Matter* **6**, 4479–4492 (1994).
33. Z.-Y. Cao, K. Zhang, A. F. Goncharov, X.-J. Yang, Z.-A. Xu, X.-J. Chen, Pressure effect of the charge density wave transition on Raman spectra and transport properties of 2*H*-$NbSe_2$. *Phys. Rev. B* **107**, 245125 (2023).
34. M. Kohler, Zur Magnetischen Widerstandsänderung Reiner Metalle. *Ann. Phys.* **424**, 211–218 (1938).
35. D. J. Rahn, S. Hellmann, M. Kalläne, C. Sohrt, T. K. Kim, L. Kipp, K. Rossnagel, Gaps and kinks in the electronic structure of the superconductor 2*H*-$NbSe_2$ from angle-resolved photoemission at 1 K. *Phys. Rev. B* **85**, 224532 (2012).
36. L.-J. Li, Z.-A. Xu, J.-Q. Shen, L.-M. Qiu, Z.-H. Gan, The effect of a charge-density wave transition on the transport properties of 2*H*-$NbSe_2$. *J. Phys. Condens. Matter* **17**, 493–498 (2005).
37. K. Cho, M. Kończykowski, S. Teknowijoyo, M. A. Tanatar, J. Guss, P. B. Gartin, J. M. Wilde, A. Kreyssig, R. J. McQueeney, A. I. Goldman, V. Mishra, P. J. Hirschfeld, R. Prozorov, Using controlled disorder to probe the interplay between charge order and superconductivity in $NbSe_2$. *Nat. Commun.* **9**, 2796 (2018).
38. W. Li, S. Pyon, A. Ichinose, S. Okayasu, T. Tamegai, Suppression of superconductivity in heavy-ion irradiated 2*H*-$NbSe_2$ caused by negative pressure. *J. Phys. Soc. Jpn.* **91**, 074709 (2022).
39. W. Li, S. Pyon, A. Yagi, T. Ren, M. Suyama, J. Wang, T. Matsumae, Y. Kobayashi, A. Takahashi, D. Miyawaki, T. Tamegai, Effects of 3 MeV proton irradiation on superconductivity and CDW in 2*H*- $NbSe_2$ single crystals. *J. Phys. Soc. Jpn.* **92**, 064701 (2023).
40. F. Flicker, J. van Wezel, Charge order from orbital-dependent coupling evidenced by $NbSe_2$. *Nat. Commun.* **6**, 7034 (2015).
41. F. Flicker, J. van Wezel, Charge order in $NbSe_2$. *Phys. Rev. B* **94**, 235135 (2016).
42. Z. Wang, C. Chen, J. Mo, J. Zhou, K. P. Loh, Y. P. Feng, Decisive role of electron-phonon coupling for phonon and electron instabilities in transition metal dichalcogenides. *Phys. Rev. Res.* **5**, 013218 (2023).
43. D. J. Huntley, R. F. Frindt, Transport properties of $NbSe_2$. *Can. J. Phys.* **52**, 74–117 (1974).
44. S. V. Borisenko, A. A. Kordyuk, V. B. Zabolotnyy, D. S. Inosov, D. Evtushinsky, B. Büchner, A. N. Yaresko, A. Varykhalov, R. Follath, W. Eberhardt, L. Patthey, H. Berger, Two energy gaps and Fermi-surface "arcs" in $NbSe_2$. *Phys. Rev. Lett.* **102**, 166402 (2009).
45. W. Shockley, Effect of magnetic fields on conduction—"Tube integrals". *Phys. Rev.* **79**, 191–192 (1950).
46. R. G. Chambers, The kinetic formulation of conduction problems. *Proc. Phys. Soc. A* **65**, 458–459 (1952).
47. H. Kontani, K. Kanki, K. Ueda, Hall effect and resistivity in high-T_c superconductors: The conserving approximation. *Phys. Rev. B* **59**, 14723–14739 (1999).
48. P. Chudzinski, M. Berben, X. Xu, N. Wakeham, B. Bernáth, C. Duffy, R. D. H. Hinlopen, Y.-T. Hsu, S. Wiedmann, P. Tinnemans, R. Jin, M. Greenblatt, N. E. Hussey, Emergent symmetry in a low dimensional superconductor on the edge of Mottness. *Science* **382**, 792–796 (2023).
49. N. Ramakrishnan, Y. T. Lai, S. Lara, M. M. Parish, S. Adam, Equivalence of effective medium and random resistor network models for disorder-induced unsaturating linear magnetoresistance. *Phys. Rev. B* **96**, 224203 (2017).
50. K. Iwaya, T. Hanaguri, A. Koizumi, K. Takaki, A. Maeda, K. Kitazawa, Electronic state of $NbSe_2$ investigated by STM/STS. *Phys. B Condens. Matter* **329-333**, 1598–1599 (2003).
51. N. V. Kozlova, N. Mori, O. Makarovsky, L. Eaves, Q. D. Zhuang, A. Krier, A. Patanè, Linear magnetoresistance due to multiple-electron scattering by low-mobility islands in an inhomogeneous conductor. *Nat. Commun.* **3**, 1097 (2012).
52. R. Peierls, Zur Theorie der elektrischen und thermischen Leitfähigkeit von Metallen. *Ann. Phys.* **396**, 121–148 (1930).
53. W. Kohn, Image of the Fermi surface in the vibration spectrum of a metal. *Phys. Rev. Lett.* **2**, 393–394 (1959).
54. M. D. Johannes, I. I. Mazin, Fermi surface nesting and the origin of charge density waves in metals. *Phys. Rev. B* **77**, 165135 (2008).
55. M. D. Johannes, I. I. Mazin, C. A. Howells, Fermi-surface nesting and the origin of the charge-density wave in $NbSe_2$. *Phys. Rev. B* **73**, 205102 (2006).
56. F. Weber, S. Rosenkranz, J.-P. Castellan, R. Osborn, R. Hott, R. Heid, K.-P. Bohnen, T. Egami, A. H. Said, D. Reznik, Extended phonon collapse and the origin of the charge-density wave in 2*H*-$NbSe_2$. *Phys. Rev. Lett.* **107**, 107403 (2011).
57. T. Valla, A. V. Fedorov, P. D. Johnson, P.-A. Glans, C. McGuinness, K. E. Smith, E. Y. Andrei, H. Berger, Quasiparticle spectra, charge density waves, superconductivity, and electron-phonon coupling in 2*H*-$NbSe_2$. *Phys. Rev. Lett.* **92**, 086401 (2004).
58. W. L. McMillan, Microscopic model of charge-density waves in 2*H*-$TaSe_2$. *Phys. Rev. B* **16**, 643–650 (1977).
59. C. M. Varma, A. L. Simons, Strong-coupling theory of charge-density-wave transitions. *Phys. Rev. Lett.* **51**, 138–141 (1983).
60. W. L. McMillan, Theory of discommensurations and the commensurate-incommensurate charge-density-wave phase transition. *Phys. Rev. B* **14**, 1496–1502 (1976).
61. A. Soumyanarayanan, M. M. Yee, Y. He, J. van Wezel, D. J. Rahn, K. Rossnagel, E. W. Hudson, M. R. Norman, J. E. Hoffman, Quantum phase transition from triangular to stripe charge order in $NbSe_2$. *Proc. Natl. Acad. Sci. U.S.A.* **110**, 1623–1627 (2013).
62. N. Doiron-Leyraud, C. Proust, D. LeBoeuf, J. Levallois, J.-B. Bonnemaison, R. Liang, D. A. Bonn, W. N. Hardy, L. Taillefer, Quantum oscillations and the Fermi surface in an underdoped high-T_c superconductor. *Nature* **447**, 565–568 (2007).
63. W. Tabis, Y. Li, M. Le Tacon, L. Braicovich, A. Kreyssig, M. Minola, G. Dellea, E. Weschke, M. J. Veit, M. Ramazanoglu, A. I. Goldman, T. Schmit, G. Ghiringhelli, N. Barišić, M. K. Chan, C. J. Dorow, G. Yu, X. Zhao, B. Keimer, M. Greven, Charge order and its connection with Fermi-liquid charge transport in a pristine high-T_c cuprate. *Nat. Commun.* **5**, 5875 (2014).
64. K. Momma, F. Izumi, *VESTA3* for three-dimensional visualization of crystal, volumetric and morphology data. *J. Appl. Crystal.* **44**, 1272–1276 (2011).
65. A. Kool, D. Pizzirani, P. Tinnemans, S. Wiedmann, F. Flicker, J. van Wezel, N. E. Hussey, R. D. H. Hinlopen, H-linear magnetoresistance in NbSe2 due to impeded cyclotron motion (2026); https://doi.org/10.34973/drd0-kj23.
66. N. P. Ong, Geometric interpretation of the weak-field Hall conductivity in two-dimensional metals with arbitrary Fermi surface. *Phys. Rev. B* **43**, 193–201 (1991).
67. H. Kontani, Optical conductivity and Hall coefficient in high-T_c superconductors: Significant role of current vertex corrections. *J. Phys. Soc. Jpn.* **75**, 013703 (2006).
68. A. B. Pippard, The influence of small-angle scattering on metallic conduction. *Proc. A* **305**, 291–318 (1968).
69. C. M. Varma, E. Abrahams, Effective Lorentz force due to small-angle impurity scattering: Magnetotransport in high-T_c superconductors. *Phys. Rev. Lett.* **86**, 4652–4655 (2001).
70. P. Knowles, B. Yang, T. Muramatsu, O. Moulding, J. Buhot, C. J. Sayers, E. Da Como, S. Friedemann, Fermi surface reconstruction and electron dynamics at the charge-density-wave transition in $TiSe_2$. *Phys. Rev. Lett.* **124**, 167602 (2020).
71. R. D. H. Hinlopen, O. N. Moulding, W. R. Broad, J. Buhot, F. Bangma, A. McCollam, J. Ayres, C. J. Sayers, E. Da Como, F. Flicker, J. van Wezel, S. Friedemann, Lifshitz transition enabling superconducting dome around a charge-order critical point. *Sci. Adv.* **10**, eadl3921 (2024).
72. R. M. Fleming, R. V. Coleman, Oscillatory magnetotransport in the layer compounds $4H_b$-TaS_2 and 2*H*-$TaSe_2$. *Phys. Rev. B* **16**, 302–315 (1977).
73. J. J. Gao, J. G. Si, X. Luo, J. Yan, Z. Z. Jiang, W. Wang, Y. Y. Han, P. Tong, W. H. Song, X. B. Zhu, Q. J. Li, W. J. Lu, Y. P. Sun, Origin of the large magnetoresistance in the candidate chiral superconductor $4H_b$-TaS_2. *Phys. Rev. B* **102**, 075138 (2020).
74. H. Chen, Z. Li, L. Guo, X. Chen, Anisotropic magneto-transport and magnetic properties of low-temperature phase of $TaTe_2$. *EPL* **117**, 27009 (2017).
75. M. Naito, S. Tanaka, Electrical transport properties in 2*H*-NbS_2, -$NbSe_2$, -TaS_2 and -$TaSe_2$. *J. Phys. Soc. Jpn.* **51**, 219–227 (1982).
76. H. Liu, L. Bao, Z. Zhou, B. Che, R. Zhang, C. Bian, R. Ma, L. Wu, H. Yang, J. Li, C. Gu, C.-M. Shen, S. Du, H.-J. Gao, Quasi-2D transport and weak antilocalization effect in few-layered VSe_2. *Nano Lett.* **19**, 4551–4559 (2019).

77. Y. Xue, Y. Zhang, H. Wang, S. Lin, Y. Li, J.-Y. Dai, S. P. Lau, Thickness-dependent magnetotransport properties in 1*T* -VSe_2 single crystals prepared by chemical vapor deposition. *Nanotechnology* **31**, 145712 (2020).
78. W. Biberacher, A. Lerf, Electrical transport properties of 2*H*-TaS_2 intercalation compounds with variable charge transfer. *Mol. Cryst. Liq. Cryst.* **121**, 149–152 (1985).
79. S. J. Hillenius, R. V. Coleman, Quantum oscillations and Fermi surface of 2*H*-TaS_2. *Phys. Rev. B* **18**, 3790–3798 (1978).
80. A. A. Sinchenko, P. D. Grigoriev, P. Lejay, P. Monceau, Linear magnetoresistance in the charge density wave state of quasi-two-dimensional rare-earth tritellurides. *Phys. Rev. B* **96**, 245129 (2017).
81. A. Fang, N. Ru, I. R. Fisher, A. Kapitulnik, STM studies of $TbTe_3$: Evidence for a fully incommensurate charge density wave. *Phys. Rev. Lett.* **99**, 046401 (2007).
82. P. Walmsley, S. Aeschlimann, J. A. W. Straquadine, P. Giraldo-Gallo, S. C. Riggs, M. K. Chan, R. D. McDonald, I. R. Fisher, Magnetic breakdown and charge density wave formation: A quantum oscillation study of the rare-earth tritellurides. *Phys. Rev. B* **102**, 045150 (2020).
83. R. Kumar, S. Singh, S. Nair, High temperature linear magnetoresistance and scaling behavior in the $Ba(Fe_{1-x}Co_x)_2As_2$ series. arXiv:1801.03768v1 [cond-mat.supr-con] (2018).
84. T. Terashima, N. Kurita, M. Kimata, M. Tomita, S. Tsuchiya, H. Satsukawa, A. Harada, K. Hazama, M. Imai, A. Sato, S. Uji, K. Kihou, C.-H. Lee, H. Kito, Y. Tomioka, T. Ito, A. Iyo, H. Eisaki, T. Liang, M. Nakajima, S. Ishida, S.-i. Uchida, T. Saito, H. Fukazawa, Y. Kohori, H. Harima, Quantum oscillations in iron-based superconductors: $BaFe_2As_2$ vs. KFe_2As_2. *J. Phys. Conf. Ser.* **449**, 012022 (2013).

Acknowledgments: We thank C. M. Duffy and J. Ayres for insightful discussions. **Funding:** This work was supported by the European Research Council (ERC) under the European Union's Horizon 2020 research and innovation programme, grant agreement no. 835279-Catch-22 (N.E.H. and R.D.H.H.); Engineering and Physical Sciences Research Council EPSRC grant EP/V02986X/1 (N.E.H.); HFML-FELIX, a member of the European Magnetic Field Laboratory (A.K., S.W., and D.P.); Engineering and Physical Sciences Research Council EPSRC (UK) via its membership of the European Magnetic Field Laboratory (grant no. EP/N01085X/1) (N.E.H.); and Engineering and Physical Sciences Research Council EPSRC grant no. EP/X012239/1 (F.F.).
Author contributions: Conceptualization: R.D.H.H. and N.E.H. Methodology: A.K., D.P., and S.W. Sample orientation: P.T. Investigation: A.K., D.P., and S.W. Data analysis: A.K. Modeling: R.D.H.H. Funding acquisition: N.E.H. and F.F. Supervision: N.E.H. Writing—original draft: A.K., R.D.H.H., and N.E.H. with key input from F.F. and J.v.W. **Competing interests:** The authors declare that they have no competing interests. **Data, code, and materials availability:** All data and code needed to evaluate and reproduce the results in the paper are present in the paper and/or the Supplementary Materials. The data and code supporting this study can be found at https://doi.org/10.34973/drd0-kj23. All new materials generated by this study are provided in Materials and Methods.

Submitted 17 July 2025
Accepted 1 April 2026
Published 29 April 2026
10.1126/sciadv.aea6029

ScienceAdvances

H-linear magnetoresistance in $NbSe_2$ due to impeded cyclotron motion

Arwin Kool, Davide Pizzirani, Paul Tinnemans, Steffen Wiedmann, Felix Flicker, Jasper van Wezel, Nigel E. Hussey, and Roemer D. H. Hinlopen

Sci. Adv. **12** (18), eaea6029. DOI: 10.1126/sciadv.aea6029

Science Advances (ISSN 2375-2548) is published by the American Association for the Advancement of Science. 1200 New York Avenue NW, Washington, DC 20005. The title *Science Advances* is a registered trademark of AAAS.